THE JOURNAL OF PHYSICAL CHEMISTRY C
A JOURNAL OF THE AMERICAN CHEMICAL SOCIETY

pubs.acs.org/JPCC

Article

Theoretical Analysis of the Electronic Structure and Optical Properties of DNA-Stabilized Silver Cluster $Ag_{16}Cl_2$ in Aqueous Solvent

Sami Malola, María Francisca Matus, and Hannu Häkkinen*

Cite This: https://doi.org/10.1021/acs.jpcc.3c04103

Read Online

ACCESS | Metrics & More | Article Recommendations | Supporting Information

ABSTRACT: DNA-stabilized silver nanoclusters with 10−30 silver atoms are by construction ideal candidates for biocompatible bright fluorescent emitters, but their electronic structure is not well understood. Here, using density functional theory (DFT), we analyze the ground-state electronic structure and optical absorption of a bright NIR-emitting cluster $Ag_{16}Cl_2$, which is stabilized by two DNA strands of 9-base sequence 5′-CACCTAGCG-3′ and whose atomic structure was very recently confirmed to have two chlorides bound to the silver core. We are able to (i) unambiguously assign the charge of this cluster in aqueous solvent, (ii) analyze the details of silver−DNA interactions and their effect on the cluster charge, (iii) analyze the character of low-energy optical absorption peaks and the involved electron orbitals and make a first assessment on circular dichroism, and (iv) evaluate the suitability of various DFT exchange−correlation functionals via benchmarking to experimental optical data. This work lays out a baseline for all future theoretical work to understand the electronic, chiroptical, and fluorescence properties of these fascinating biocompatible nanostructures.

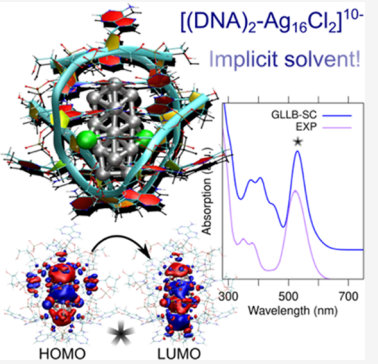

1. INTRODUCTION

Small metal clusters stabilized by ligand molecules confine a discrete number of delocalized valence electrons to their inorganic core, which leads to a quantized electronic structure and distinct optical properties.[1] These properties are highly sensitive to the metal type, ligand type, cluster size, and cluster shape, creating a possibility to tune the optical response such as the intensity and wavelength of fluorescence by changing the chemical parameters in the synthesis. Tunable quantum characteristics combined with the functionalization possibilities have made these systems unique for various different applications, from which biolabeling and biosensing are one of the most exciting subfields.[2] For almost two decades, DNA-templated silver clusters having up to about 30 silver atoms have been demonstrated as bright emitters in the visible to near-infrared (NIR) range of wavelengths controlled by the selected DNA sequence.[3−16] Theoretical studies on this intriguing phenomenon have been limited due to the absence of solid experimental evidence on the atomic structures of such clusters, although model studies on small silver−DNA complexes have produced important information of interactions between silver cations and different DNA bases.[17−21] The field took important steps forward when crystal structures of two DNA-templated silver clusters (Ag_8 and Ag_{16}) were reported in 2019.[6,22] The rod-like and geometrically slightly chiral Ag_{16} cluster,[22] templated by two DNA strands (each strand has the 10-base sequence 5′-CACCTAGCGA-3′), is particularly interesting since it is fluorescent in the NIR region and has a large Stokes shift. Very recently, reanalysis of this cluster by means of electrospray ionization mass spectrometry, nuclear magnetic spectroscopy (NMR), density functional theory (DFT) calculations, and refined single-crystal X-ray analysis discovered that the 16-atom silver core has two chlorides bound to it.[23] The two Cl sites had been previously assigned as partially occupied silver sites.[22] Our preliminary DFT calculations provided a rather good description of the optical absorption of the $(DNA)_2$−$Ag_{16}Cl_2$ cluster and helped to interpret the NMR data.

The firm knowledge of the crystal structure of the $(DNA)_2$−$Ag_{16}Cl_2$ allows now for more detailed theoretical DFT analysis, paving ways to better understanding of the structure−property relations of these materials. Here, we expand our previous theoretical investigations[23] based on the A10-variant[24] of the $(DNA)_2$−$Ag_{16}Cl_2$ cluster (Figure 1a). Our DFT calculations are able to unambiguously determine the natural charge state of the complex in the solvent, derived from the electronic stability of the silver core having a six-free-electron configuration. We highlight an important role of a specific guanine−silver interaction contributing to the total charge. We show an excellent agreement between computed and measured optical absorption data allowing us to interpret the character of

Received: June 18, 2023
Revised: July 27, 2023

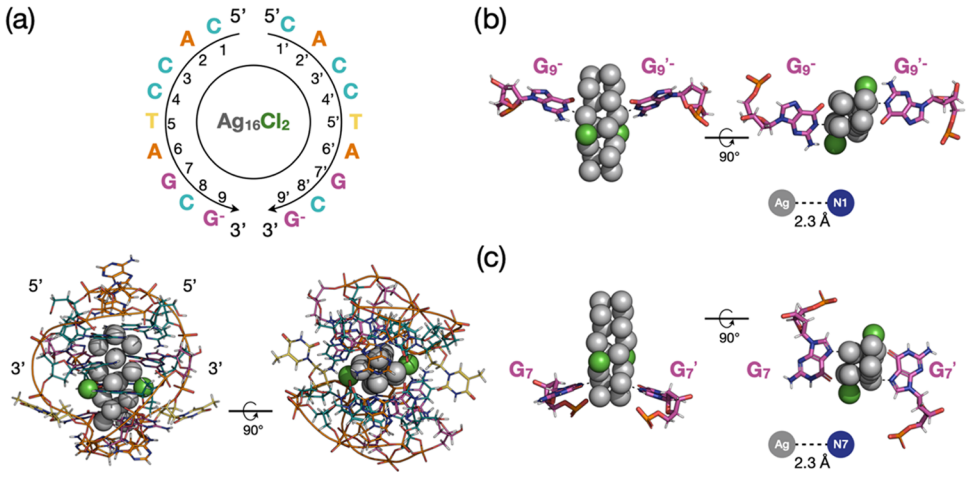

Figure 1. Structure of the A10-variant of the $(DNA)_2$−$Ag_{16}Cl_2$ cluster. (a) Schematic drawing and 3D structure (side and top views) of the DNA-stabilized cluster (PDB accession code: 6M2P) showing the distribution of the nucleobases around the inorganic core (gray, Ag; green, Cl). (b) Side and top views of the interaction between the deprotonated guanine G_9^- and the silver atoms. (c) Side and top views of the interaction between the neutral guanine G_7 and the silver atoms.

the low-energy absorption peaks in detail in terms of electron−hole excitations and contributions from the silver core and DNA strands also determining the origin of circular dichroism (CD). We explore the electronic structure with a variety of electronic exchange−correlation functionals and are able to benchmark the most reliable functional against experimental data, laying groundwork for further theoretical investigations of electronic, optical, chiral, and fluorescence properties of these materials. The necessary next steps are discussed.

2. COMPUTATIONAL METHODS

The DFT calculations were done with the GPAW software, which uses real-space grids for solving for the ground-state electronic structure.[25] A 0.30 Å grid spacing was used with PBE[26] and GLLB-SC[27] exchange−correlation functionals, whereas 0.25 Å grid spacing was used with LB94[28] and CAMH-B3LYP[29] functionals. The grid spacings were chosen to find a reasonable balance between accuracy and computational efficiency. A vacuum layer of 6 Å was used around the system in all cases. The PAW atomic setups of the Ag atom were done at the scalar-relativistic level. The wavefunctions of the ground state were solved using the experimental crystal structure[23,24] as is, together with the implicit continuum solvent model and a total charge of −10 |e| with all functionals. For comparison, the electronic structure was solved also using −8 |e| total charge with the PBE functional. The parameters of the continuum solvent model were selected for water as in the work by Walter et al.,[30] which includes a detailed discussion of the model. The electron states were decomposed to contributions by different atoms by projecting the density of states to spherical harmonics inside a spherical volume around each atom.[31] Summation was taken over all of the angular momenta and over the specified atoms for determining the final weights of the localization. The cutoff radii of the elements were as follows: Ag: 1.5 Å, Cl: 1.3 Å, P: 0.8 Å, O: 0.7 Å, C: 0.7 Å, N: 0.7 Å, H: 0.5 Å.

Optical absorption and circular dichroism spectra were calculated starting from the ground-state wavefunctions (solved with the continuum solvent model) using linear response time-dependent density functional theory (LR-TDDFT).[32] PBE, LB94, and LDA functionals were used as the TDDFT kernel, but we observed almost identical UV−vis spectra independent of the functional and report the main results using the PBE as the kernel. In LR-TDDFT, the xc-kernel forms the interacting part by adding exchange and correlation effects to the response over the noninteracting response using Kohn−Sham states. We also note that the GLLB-SC functional cannot be used as the kernel since density gradients cannot be calculated. The GLLB-SC functional is known to give a larger Kohn−Sham energy gap of the protected metal nanoclusters than PBE and was developed originally as an efficient method for improved description of band gaps in semiconductor materials.[27] The continuum solvent model was used also in calculating the particle−hole excitations. Our approach is missing such transitions where explicit solvent molecules might contribute, but such limitation might become relevant only in the high-UV region at the DNA−water interface, outside the energy range considered in this work. Individual oscillator strengths (for absorption) and rotatory strengths (for CD) were smoothened out by 0.1 eV Gaussians and summed up for continuous curves. Peaks of the optical absorption spectra were analyzed for the GLLB-SC spectrum using dipole transition contribution maps (DTCM) that were calculated with time-dependent density functional perturbation theory (TD-DFPT).[33] DTCM shows the constructive and screening contributions to the total dipole transition moment at the selected energy in the Kohn−Sham (ground-state) electron−hole basis. DTCMs are shown here as total plots including analysis in all of the three Cartesian coordinate directions of the polarization of the electric field, which were aligned with the principal axis of the moments of inertia of the system. TD-DFPT was also used to solve the electron−hole densities and the induced densities at the peak energies. Electron−hole and induced densities were analyzed with respect to the main axis of the cluster. Local charges of atoms and atom groups were analyzed using the Bader charge method.[34]

3. RESULTS AND DISCUSSION

Our preliminary DFT calculations[23] employed the PBE exchange−correlation functional[26] treating $(DNA)_2$−$Ag_{16}Cl_2$ as an isolated complex in the gas phase with the total charge

https://doi.org/10.1021/acs.jpcc.3c04103
J. Phys. Chem. C XXXX, XXX, XXX−XXX

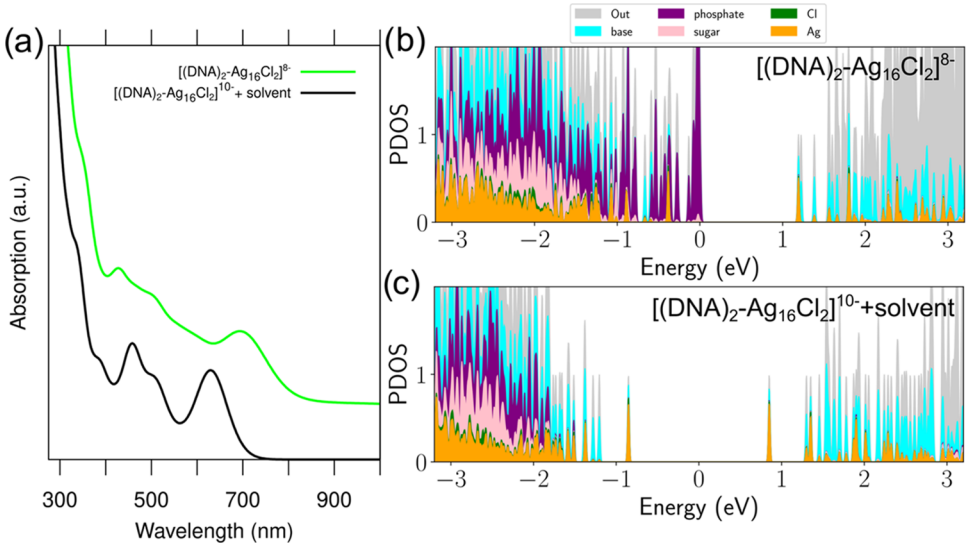

Figure 2. (a) Comparison of calculated optical absorption spectra of $[(DNA)_2{-}Ag_{16}Cl_2]^{8-}$ without implicit solvent (green line) and $[(DNA)_2{-}Ag_{16}Cl_2]^{10-}$ with implicit solvent (black line) using the PBE functional. (b, c) Projected density of electronic states (PDOS) to atom orbitals of Ag, Cl, base, sugar, and phosphate groups for the same systems. Coloring denotes the total weights on the specified atom groups. "Out" denotes weights from spatial distribution of electrons that is not captured by the analysis. In (b), the HOMO state at zero energy is partially occupied (degeneracy of states) and the first fully empty orbital lies at 1.19 eV. In (c), the HOMO−LUMO energy gap (1.70 eV) is centered around zero and the HOMO state is fully occupied.

matching the expected configuration of six "free" electrons in the silver core. This amounts to a charge of −8 lel based on 16 negatively charged phosphate groups, 16 donated Ag(s) electrons, and two electron-withdrawing chlorides; *i.e.*, the net count of electrons is 6 (= 8−16 + 16−2). This model gave an optical absorption spectrum that qualitatively agreed with the measured data, specifically, a clear lowest-energy peak at 694 nm and two weak higher-energy signals around 400−500 nm (Figure 2a), although all of these peaks were significantly red-shifted with respect to the experiment.[23] The character of the lowest-energy peak was analyzed in terms of single electron−hole transitions and induced dipole density that showed clear longitudinal excitations along the silver core. Minor contributions from the phosphate groups were also observed in the induced dipole density. This was assigned tentatively due to the missing dielectric environment as no solvent was modeled. The potential solvent effects were not investigated further as our efforts concentrated on interpreting the ^{35}Cl NMR spectra, being an important part of producing evidence for the existence of the chlorides in the silver core.[23]

3.1. Optimal Charge State in the Solvent. Our new work concentrated first on a detailed analysis of the character of electronic states of $(DNA)_2{-}Ag_{16}Cl_2$ with −8 lel charge without the solvent using the PBE functional. As Figure 2b shows, the phosphate contributions show up strongly also in the density of electron states when they are projected (PDOS) onto the natural components of the system (silver, chloride, base, sugar, and phosphate), creating partially occupied states close to the energy of the highest occupied molecular orbital (HOMO). This explains their activity also in the low-lying optical absorption. We then repeated the calculation with the implicit water solvent model and observed that the phosphate states moved down to more negative energies (*i.e.*, were stabilized by the solvent) as expected; however, the degenerate HOMO/LUMO state remained displaying a two-electron hole (not shown here). This fact indicated that the used −8 lel total charge was not optimal, but there would be added electronic stability of the compound for −10 lel charge due to opening of a large HOMO−LUMO energy gap at that charge in the PDOS (Figure 2c). With that charge and using the solvent model, the shape of the optical absorption spectrum remained similar as compared to $[(DNA)_2{-}Ag_{16}Cl_2]^{8-}$ without solvent, but the lowest-energy absorption peak of $[(DNA)_2{-}Ag_{16}Cl_2]^{10-}$ blue-shifted by 65 nm, giving a better agreement with the experimental data (Figure 2a).

The chemical argument to add two additional electrons in the model (increasing the charge of the complex to −10 lel) is found by examining the silver−DNA interface in the crystal structure data of the A10-variant.[24] As Figures 1 and S1 show, there are two guanines, G_7 and G_9, interacting with silver on both sides of the $Ag_{16}Cl_2$ core. Remarkably, while G_7 is found in the neutral form, G_9 is deprotonated at the N1 position (G_9^-), but both N7(G_7)−Ag and N1(G_9^-)−Ag distances are the same (about 2.3 Å) (Figure 1b,c). The N1(G_9^-)−Ag interactions form the grounds for the added electronic charge. The interaction between neutral guanine and silver cations through the N7 atom and the neighboring carbonyl group (C6 position) has been documented in the literature to be the most stable position for the metallobase pair.[35,36] However, different protonation states of the same nucleobase can coexist within the same metal−DNA complex. This interesting phenomenon is not yet fully understood, but it has been reported that it could be due to a perturbation of silver on the charge distribution (shifting of pK_a values) of the nucleobases.[37] Similar to how metal cations induce deprotonation of guanine at the N1 position in ribozymes,[38] silver could cause acidification of the NH groups of G_9, suggesting that there are different microenvironments inside $[(DNA)_2{-}Ag_{16}Cl_2]^{10-}$. Bader charges for silver atoms interacting with N7(G_7) and N1(G_9^-) are similar (0.393 and 0.383 lel vs 0.377 and 0.369 lel, respectively; Figure S1), but the environment of G_7 and G_9^- is different in terms of hydrogen bonds contribution and pi-stacking interactions established with their neighboring bases. In both strands, G_7 forms hydrogen bonds with T_5 and pi-

https://doi.org/10.1021/acs.jpcc.3c04103
J. Phys. Chem. C XXXX, XXX, XXX−XXX

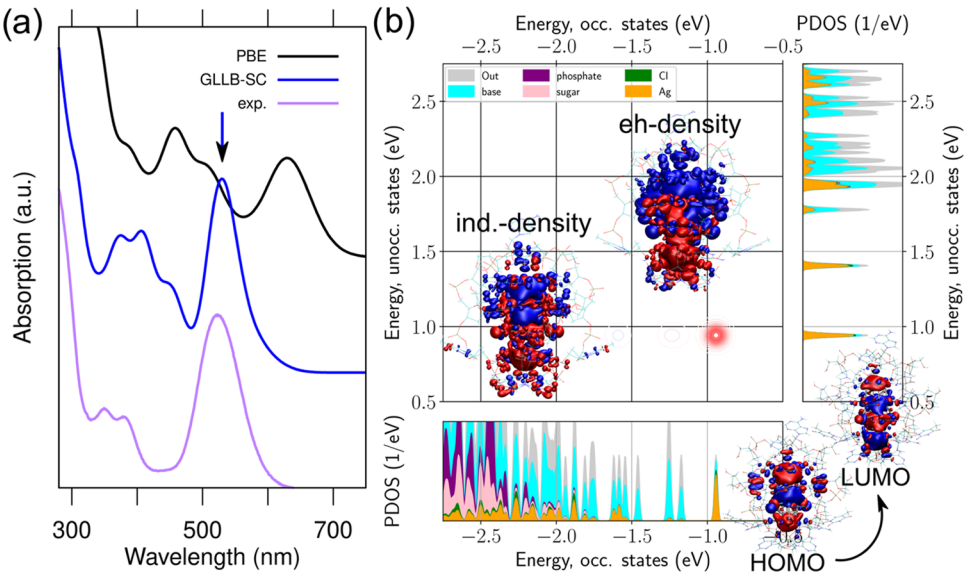

Figure 3. (a) Comparison of experimental and calculated (implicit solvent, PBE, and GLLB-SC functionals used for the electronic ground state) absorption spectra of the $[(DNA)_2{-}Ag_{16}Cl_2]^{10-}$ cluster, (b) dipole transition contribution map (DTCM), induced density, and electron−hole density for the lowest energy absorption peak of the absorption spectrum (GLLB-SC ground state) at 530 nm (the blue arrow in panel a). In the DTCM plot, the red spot in the top left panel indicates the single HOMO → LUMO transition being responsible for this peak. The projected densities of occupied and unoccupied states (PDOS) are shown in the bottom left and top right panels, respectively. The projection is done as in Figure 2. Electron−hole density and the induced density are shown on top of the DTCM plot.

stacking interactions with A_6 and C_8, while G_9^- forms hydrogen bonds with C_4 and pi-stacking interactions only with C_1, being more exposed to the solvent. In fact, it is observed in the crystal structure (PDB ID: 6M2P) that G_9^- forms multiple hydrogen bonds with three or even six water molecules, while only one water molecule is found near G_7, which indicates that a synergy of hydration and base stacking dictates the metal-mediated deprotonation of specific nucleobases. Overall, atomic Bader charges summed up to the natural components of the system follow an expected pattern where the silver atoms and sugar groups are positively charged and chlorides, bases, and phosphates are negatively charged (Table S1).

3.2. Performance of Exchange−Correlation Functionals. We then employed three other exchange−correlation functionals to calculate the electronic ground state of $[(DNA)_2 - Ag_{16}]^{10-}$ in solvent, GLLB-SC,[27] LB94,[28] and CAMH-B3LYP,[29] and recalculated the optical spectra by using the PBE functional in the exchange−correlation kernel (see the Methods section and Figures S2 and S3). We found that the character of the frontier orbitals remains largely the same, independent of the functional except in the case for CAMH-B3LYP where the LUMO state having weight on silver is next to a continuous band of empty states (Figure S2). However, the functional by which the ground state was calculated has a clear effect on the optical spectrum (Figure S3). The HOMO−LUMO energy gap depends somewhat on the functional as follows: 1.70 eV (PBE), 1.68 eV (LB94), 1.88 eV (GLLB-SC), and 1.53 eV (CAMH-B3LYP). The largest energy gap produced by GLLB-SC gave a reason to expect a further blue shift of the lowest-energy absorption peak, which indeed turned out to be the case (Figures 3a and S3). Figure 3a compares the computed results with PBE and GLLB-SC in reference to the experimental data. Remarkably, the spectrum computed by using the GLLB-SC functional for the ground state shows an excellent agreement with the experiment as the lowest-energy peak is clearly the most intensive one in the region of 350−550 nm and its position at 530 nm is very close to the experimental value at 522 nm. The peaks at 375 and 407 nm are close to the ones regularly seen in the experimental data,[23] and a very recent study[39] also reported a weak signal close to our computed peak at 449 nm. We wish to stress here that the choice of the functional for solving the ground-state electron density is indeed the critical one, since choice of the exchange−correlation kernel in the LR-TDDFT calculations has a negligible effect on the absorption spectra (Figure S4).

3.3. Analysis of the Optical Spectrum and Frontier Orbitals. We then analyzed the character of all four peaks mentioned above by creating the corresponding dipole transition contribution maps[33] (Figures 3b and S5). The lowest-energy peak at 530 nm is clearly a single orbital transition of HOMO → LUMO (silver → silver) character, without any collective contributions from other states (Figure 3b). This unambiguously clarifies the nature of this intense transition, which is sometimes hypothesized as being of collective or "plasmonic" character. The three weaker peaks at 449, 407, and 375 nm are more collective (Figure S5), having contributions both from the HOMO → LUMO transition and from silver → base and base → silver transitions.

We visualize the frontier orbitals from HOMO-7 to LUMO + 3 in Figure 4. Most of these orbitals have a major weight in the inorganic silver−chloride core except HOMO-(3,2,1). HOMO-1 and HOMO-2 are localized on the deprotonated G_9^- on each DNA strand (second and first strands, respectively), while HOMO-3 is localized on A_2'. Orbitals that are localized in the inorganic core follow systematic particle-in-a-box symmetries, with HOMO-(7,6) having one node plane in the "silver box" perpendicular to the longitudinal direction, HOMO having two node planes, LUMO having three node planes, and LUMO + (1,2,3) having node planes in the transverse direction. The symmetry analysis reinforces the picture of a strong dipole-allowed HOMO → LUMO longitudinal transition, which indeed is seen in Figure 3b.

https://doi.org/10.1021/acs.jpcc.3c04103
J. Phys. Chem. C XXXX, XXX, XXX−XXX

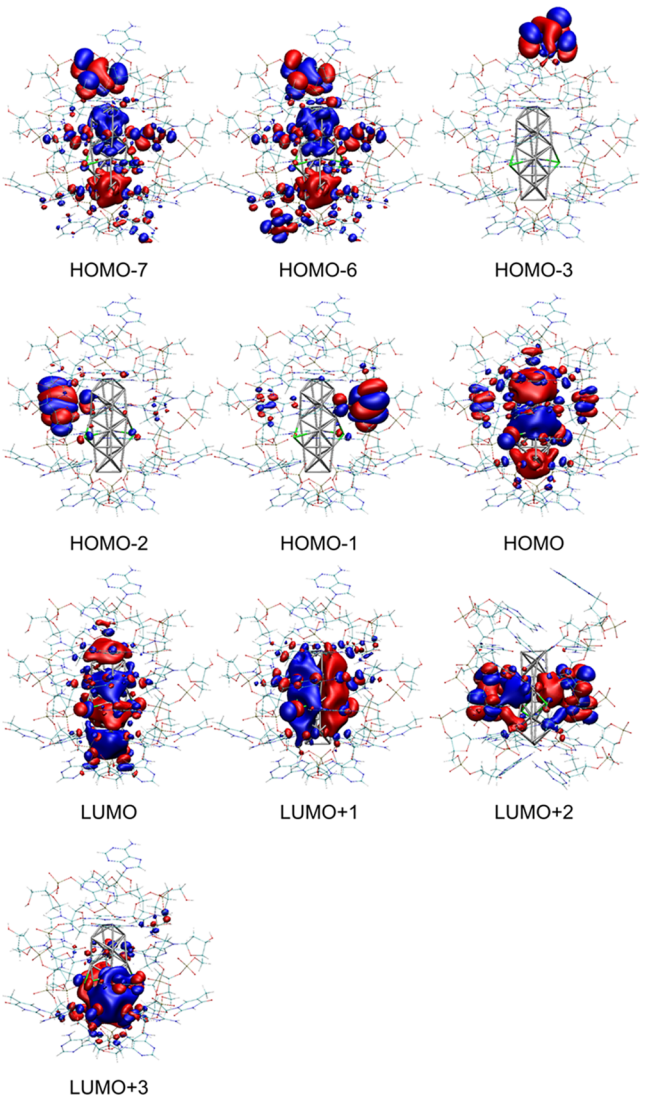

Figure 4. Visualized frontier molecular orbitals of the $[(DNA)_2-Ag_{16}Cl_2]^{10-}$ cluster calculated with the GLLB-SC functional and implicit solvent.

It is interesting to note that the LUMO orbital that is localized mostly in the silver core is active in all of the analyzed absorption peaks, but in some peaks also higher-lying empty orbitals are involved. This implies that the details of the electronic relaxation processes should depend on the excitation energy. Although we do not intend to study the fluorescence in this work, one can assume that in the first approximation, similar orbitals (HOMO and LUMO) that are responsible for the lowest-energy absorption also play a role in the fluorescence after electronic relaxation. This gives a rather simple framework to understand the size dependence of the absorption and fluorescence on DNA–Ag cluster materials having the elongated shape of the inorganic core, well documented experimentally.[12,13,40,41] If the absorption and fluorescence are realistically described by one-electron transition, the physics can be drawn from simple electron-in-a-box model, where the energy of the lowest transition should follow 1/L behavior (L is the box length). In fact, we have documented this physics previously in another cluster model where we built linear chains of thiolate-protected gold nanoclusters up to an aspect ratio of 1:6 and showed a strong red shift and intensity increase (due to the increased transition dipole) in the VIS–NIR absorption as the length of the system increased.[42] Silver nanowires also show this behavior as the energetic separation of Ag(4d) and Ag(5s) electrons is large and the low-energy optical absorption can be understood well from a monovalent "jellium rod model".[43]

3.4. Circular Dichroism. The excellent agreement between the measured data and the computed linear absorption of the $[(DNA)_2 - Ag_{16}]^{10-}$ cluster with the GLLB-SC functional in the solvent model encouraged us to calculate the CD spectrum, which shows the differences in linear absorption due to different handedness of circularly polarized light. Figure 5 compares the CD spectrum with the linear absorption

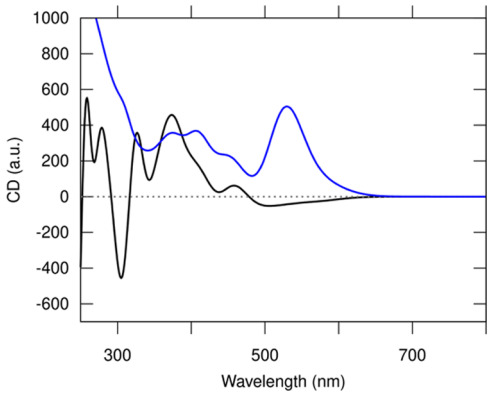

Figure 5. Circular dichroism (CD) spectrum (black) and the linear absorption spectrum (blue) of the $[(DNA)_2–Ag_{16}Cl_2]^{10-}$ cluster calculated with the implicit solvent model, GLLB-SC functional for the electronic ground state, and PBE functional for the LR-TDDFT kernel. For comparison, spectra calculated with the PBE functional for charge states 8 and 10 are shown in Figure S6.

spectrum. Several positive (+) and negative (−) peaks can be identified, forming a "fingerprint" of this structure in our model. The first − and + features in the 450–550 nm range are weak, complying with the facts that in this range the silver–silver transitions dominate, and the silver core has only very weak chiral distortion (Figure 1b,c). The signals get stronger toward higher absorption energies, where the DNA bases first start to be active and indirectly also affect the metal transitions. Currently, our results serve as a first theoretical prediction since the experimental CD data is not available for comparisons.

4. CONCLUSIONS

Our results clearly point out that any realistic DFT calculations of DNA–silver cluster complexes must consider the appropriate intrinsic charge in solvent and the solvent environment is needed to be described at least in a minimal (implicit) model like the one used here. Among the electronic exchange–correlation functionals tested in this work, the GLLB-SC functional seems to work best to characterize the ground-state electronic structure as judged from the optical absorption spectrum. Although we have been able to use, for the first time, high-resolution crystal structure data to draw realistic atom-scale models of DNA–silver clusters for DFT investigations of their electronic structure, optical properties, and circular dichroism, several issues are worth investigating further. Among them is the question how sensitive these properties are to small deviations from the crystal structure, induced by

https://doi.org/10.1021/acs.jpcc.3c04103
J. Phys. Chem. C XXXX, XXX, XXX–XXX

computationally optimized models (different exchange−correlation functionals lead to slightly different optimized atomic bonds) or by temperature-dependent dynamical effects. For finding the optimal balance between the accuracy of the xc-functional and the precise atomic and electronic structures, the dispersion corrections could be relevant to test in the future. Long-time-scale dynamic studies of these systems will pose a numerical challenge at any DFT level; consequently, reliable classical force fields for the silver−chloride core and its interactions with DNA are needed but are not currently available. This may prove to be especially important for successful attempts to understand the chiroptical response of these materials.[11,44] Long-time-scale classical molecular dynamics simulations in water may reveal the fluxionality of the inorganic core and core−DNA interactions that are likely to affect many details of the computed CD spectrum. Other cluster sizes and different cluster shapes will undoubtedly change the characteristics of the electronic structure and (chir)optical response, which will form an interesting challenge for atom-scale theory of these intriguing materials.

■ ASSOCIATED CONTENT

Supporting Information

The Supporting Information is available free of charge at https://pubs.acs.org/doi/10.1021/acs.jpcc.3c04103.

Additional analysis of the electronic structure, optical spectrum, and the silver−DNA interface of the $[(DNA)_2 - Ag_{16}]^{10-}$ cluster (PDF)

■ AUTHOR INFORMATION

Corresponding Author

Hannu Häkkinen − *Department of Physics, Nanoscience Center, University of Jyväskylä, FI-40014 Jyväskylä, Finland; Department of Chemistry, Nanoscience Center, University of Jyväskylä, FI-40014 Jyväskylä, Finland;* orcid.org/0000-0002-8558-5436; Email: hannu.j.hakkinen@jyu.fi

Authors

Sami Malola − *Department of Physics, Nanoscience Center, University of Jyväskylä, FI-40014 Jyväskylä, Finland*

María Francisca Matus − *Department of Physics, Nanoscience Center, University of Jyväskylä, FI-40014 Jyväskylä, Finland;* orcid.org/0000-0002-4816-531X

Complete contact information is available at: https://pubs.acs.org/10.1021/acs.jpcc.3c04103

Notes

The authors declare no competing financial interest.

■ ACKNOWLEDGMENTS

We thank Stacy Copp, Anna Gonzàlez-Rosell, and Tom Vosch for several illuminating discussions on the properties of DNA-stabilized silver clusters. This work was supported by the Academy of Finland and by the Excellence Funding from the JYU Rector. The computations were made at the Finnish national supercomputing center CSC.

■ REFERENCES

(1) Häkkinen, H. Electronic Shell Structures in Bare and Protected Metal Nanoclusters. *Adv. Phys. X* **2016**, *1*, 467−491.

(2) Matus, M. F.; Häkkinen, H. Understanding ligand-protected noble metal nanoclusters at work. *Nat. Rev. Mater.* **2023**, *8*, 372−389.

(3) Petty, J. T.; Zheng, J.; Hud, N. V.; Dickson, R. M. DNA-Templated Ag Nanocluster Formation. *J. Am. Chem. Soc.* **2004**, *126*, 5207−5212.

(4) Chen, Y.; Phipps, M. L.; Werner, J. H.; Chakraborty, S.; Martinez, J. S. DNA Templated Metal Nanoclusters: From Emergent Properties to Unique Applications. *Acc. Chem. Res.* **2018**, *51*, 2756−2763.

(5) Gonzàlez-Rosell, A.; Cerretani, C.; Mastracco, P.; Vosch, T.; Copp, S. M. Structure and Luminescence of DNA-Templated Silver Clusters. *Nanoscale Adv.* **2021**, *3*, 1230−1260.

(6) Huard, D. J. E.; Demissie, A.; Kim, D.; Lewis, D.; Dickson, R. M.; Petty, J. T.; Lieberman, R. L. Atomic Structure of a Fluorescent Ag8 Cluster Templated by a Multistranded DNA Scaffold. *J. Am. Chem. Soc.* **2019**, *141*, 11465−11470.

(7) Mastracco, P.; Gonzàlez-Rosell, A.; Evans, J.; Bogdanov, P.; Copp, S. M. Chemistry-Informed Machine Learning Enables Discovery of DNA-Stabilized Silver Nanoclusters with Near-Infrared Fluorescence. *ACS Nano* **2022**, *16*, 16322−16331.

(8) Vosch, T.; Antoku, Y.; Hsiang, J.-C.; Richards, C. I.; Gonzalez, J. I.; Dickson, R. M. Strongly Emissive Individual DNA-Encapsulated Ag Nanoclusters as Single-Molecule Fluorophores. *Proc. Natl. Acad. Sci. U.S. A.* **2007**, *104*, 12616−12621.

(9) Petty, J. T.; Carnahan, S.; Kim, D.; Lewis, D. Long-Lived Ag106 + Luminescence and a Split DNA Scaffold. *J. Chem. Phys.* **2021**, *154*, No. 244302.

(10) Rück, V.; Cerretani, C.; Neacşu, V. A.; Liisberg, M. B.; Vosch, T. Observation of Microsecond Luminescence While Studying Two DNA-Stabilized Silver Nanoclusters Emitting in the 800−900 Nm Range. *Phys. Chem. Chem. Phys.* **2021**, *23*, 13483−13489.

(11) Gonzàlez-Rosell, A.; Guha, R.; Cerretani, C.; Rück, V.; Liisberg, M. B.; Katz, B. B.; Vosch, T.; Copp, S. M. DNA Stabilizes Eight-Electron Superatom Silver Nanoclusters with Broadband Down-conversion and Microsecond-Lived Luminescence. *J. Phys. Chem. Lett.* **2022**, *13*, 8305−8311.

(12) Schultz, D.; Gardner, K.; Oemrawsingh, S. S. R.; Markeševič, N.; Olsson, K.; Debord, M.; Bouwmeester, D.; Gwinn, E. Evidence for Rod-Shaped DNA-Stabilized Silver Nanocluster Emitters. *Adv. Mater.* **2013**, *25*, 2797−2803.

(13) Copp, S. M.; Schultz, D.; Swasey, S. M.; Faris, A.; Gwinn, E. G. Cluster Plasmonics: Dielectric and Shape Effects on DNA-Stabilized Silver Clusters. *Nano Lett.* **2016**, *16*, 3594−3599.

(14) Neacşu, V. A.; Cerretani, C.; Liisberg, M.; Swasey, S. M.; Gwinn, E. G.; Copp, S. M.; Vosch, T. Unusually Large Fluorescence Quantum Yield for a Near-Infrared Emitting DNA-Stabilized Silver Nanocluster. *Chem. Commun* **2020**, *56*, 6384.

(15) Gwinn, E. G.; O'Neill, P.; Guerrero, A. J.; Bouwmeester, D.; Fygenson, D. K. Sequence-Dependent Fluorescence of DNA-Hosted Silver Nanoclusters. *Adv. Mater.* **2008**, *20*, 279−283.

(16) Schultz, D.; Gwinn, E. G. Silver Atom and Strand Numbers in Fluorescent and Dark Ag:DNAs. *Chem. Commun.* **2012**, *48*, 5748−5750.

(17) Espinosa Leal, L. A.; Karpenko, A.; Swasey, S.; Gwinn, E. G.; Rojas-Cervellera, V.; Rovira, C.; Lopez-Acevedo, O. The Role of Hydrogen Bonds in the Stabilization of Silver-Mediated Cytosine Tetramers. *J. Phys. Chem. Lett.* **2015**, *6*, 4061.

(18) Chen, X.; Karpenkov, A.; Lopez-Acevedo, O. Silver-Mediated Double Helix: Structural Parameters for a Robust DNA Building Block. *ACS Omega* **2017**, *2*, 7343−7348.

(19) Chen, X.; Makkonen, E.; Golze, D.; Lopez-Acevedo, O. Silver-Stabilized Guanine Duplex: Structural and Optical Properties. *J. Phys. Chem. Lett.* **2018**, *9*, 4789.

(20) Chen, X.; Boero, M.; Lopez-Acevedo, O. Atomic Structure and Origin of Chirality of DNA-Stabilized Silver Clusters. *Phys. Rev. Materials* **2020**, *4*, No. 065601.

(21) Buceta, D.; Busto, N.; Barone, G.; Leal, J. M.; Domínguez, F.; Giovanetti, L. J.; Requejo, F. G.; García, B.; López-Quintela, M. A. (2015), Ag2 and Ag3 Clusters: Synthesis, Characterization, and Interaction with DNA. *Angew. Chem., Int. Ed.* **2015**, *54*, 7612−7616.

(22) Cerretani, C.; Kanazawa, H.; Vosch, T.; Kondo, J. Crystal Structure of a NIR-Emitting DNA-Stabilized Ag_{16} Nanocluster. *Angew. Chem., Int. Ed.* **2019**, *58*, 17153−17157.
(23) Gonzàlez-Rosell, A.; Malola, S.; Guha, R.; Arevalos, N. R.; Matus, M. F.; Goulet, M. E.; Haapaniemi, E.; Katz, B. B.; Vosch, T.; Kondo, J.; et al. Chloride Ligands on DNA-Stabilized Silver Nanoclusters. *J. Am. Chem. Soc.* **2023**, *145*, 10721−10729.
(24) Cerretani, C.; Kondo, J.; Vosch, T. Removal of the A10 Adenosine in a DNA-Stabilized Ag16 Nanocluster. *RSC Adv.* **2020**, *10*, 23854−23860.
(25) Enkovaara, J.; Rostgaard, C.; Mortensen, J. J.; Chen, J.; Dułak, M.; Ferrighi, L.; Gavnholt, J.; Glinsvad, C.; Haikola, V.; Hansen, H. A.; et al. Electronic Structure Calculations with GPAW: A Real-Space Implementation of the Projector Augmented-Wave Method. *J. Phys.: Condens. Matter* **2010**, *22*, No. 253202.
(26) Perdew, J. P.; Burke, K.; Ernzerhof, M. Generalized Gradient Approximation Made Simple. *Phys. Rev. Lett.* **1996**, *77*, 3865−3868.
(27) Kuisma, M.; Ojanen, J.; Enkovaara, J.; Rantala, T. T. Kohn-Sham Potential with Discontinuity for Band Gap Materials. *Phys. Rev. B* **2010**, *82*, No. 115106.
(28) van Leeuwen, R.; Baerends, E. J. Exchange-Correlation Potential with Correct Asymptotic Behavior. *Phys. Rev. A* **1994**, *49*, 2421.
(29) Shao, Y.; Mei, Y.; Sundholm, D.; Kaila, V. R. I. Benchmarking the Performance of Time-Dependent Density Functional Theory Methods on Biochromophores. *J. Chem. Theory Comput.* **2020**, *16*, 587−600.
(30) Held, A.; Walter, M. Simplified Continuum Solvent Model with a Smooth Cavity Based on Volumetric Data. *J. Chem. Phys.* **2014**, *141*, No. 174108.
(31) Walter, M.; Akola, J.; Lopez-Acevedo, O.; Jadzinsky, P. D.; Calero, G.; Ackerson, C. J.; Whetten, R. L.; Grönbeck, H.; Häkkinen, H. A Unified View of Ligand-Protected Gold Clusters as Superatom Complexes. *Proc. Natl. Acad. Sci. U.S.A.* **2008**, *105*, 9157−9162.
(32) Walter, M.; Häkkinen, H.; Lehtovaara, L.; Puska, M.; Enkovaara, J.; Rostgaard, C.; Mortensen, J. J. Time-Dependent Density-Functional Theory in the Projector Augmented-Wave Method. *J. Chem. Phys.* **2008**, *128*, No. 244101.
(33) Malola, S.; Lehtovaara, L.; Enkovaara, J.; Häkkinen, H. Birth of the Localized Surface Plasmon Resonance in Monolayer-Protected Gold Nanoclusters. *ACS Nano* **2013**, *7*, 10263−10270.
(34) Tang, W.; Sanville, E.; Henkelman, G. A Grid-Based Bader Analysis Algorithm without Lattice Bias. *J. Phys. Condens Matter.* **2009**, *21*, No. 084204.
(35) Swasey, S. M.; Leal, L. E.; Lopez-Acevedo, O.; Pavlovich, J.; Gwinn, E. G. Silver (I) as DNA Glue: Ag+-Mediated Guanine Pairing Revealed by Removing Watson-Crick Constraints. *Sci. Rep.* **2015**, *5*, No. 10163.
(36) Dale, B. B.; Senanayake, R. D.; Aikens, C. M. Research Update: Density Functional Theory Investigation of the Interactions of Silver Nanoclusters with Guanine. *APL Mater.* **2017**, *5*, No. 053102.
(37) David, F.; Setzler, C.; Sorescu, A.; Lieberman, R. L.; Meilleur, F.; Petty, J. T. Mapping H + in the Nanoscale (A2C4) 2-Ag8 Fluorophore. *J Phys Chem Lett* **2022**, *13*, 11317−11322.
(38) Lippert, B. Ligand-pKa Shifts through Metals: Potential Relevance to Ribozyme Chemistry. *Chem. Biodiversity* **2008**, *5*, 1455−1474.
(39) Chen, J.; Kumar, A.; Cerretani, C.; Vosch, T.; Zigmantas, D.; Thyrhaug, E. Excited-State Dynamics in a DNA-Stabilized Ag16 Cluster with Near-Infrared Emission. *J. Phys. Chem. Lett.* **2023**, *14*, 4078−4083.
(40) Copp, S. M.; Schultz, D.; Swasey, S.; Pavlovich, J.; Debord, M.; Chiu, A.; Olsson, K.; Gwinn, E. Magic Numbers in DNA-Stabilized Fluorescent Silver Clusters Lead to Magic Colors. *J. Phys. Chem. Lett.* **2014**, *5*, 959−963.
(41) Copp, S. M.; Gonzàlez-Rosell, A. Large-Scale Investigation of the Effects of Nucleobase Sequence on Fluorescence Excitation and Stokes Shifts of DNA-Stabilized Silver Clusters. *Nanoscale* **2021**, *13*, 4602−4613.
(42) Malola, S.; Lehtovaara, L.; Häkkinen, H. A DFT Study of Linear Gold-Thiolate Superclusters Absorbing in the Therapeutic NIR Window. *J. Phys. Chem. Lett.* **2014**, *5*, 1329.
(43) Guidez, E. B.; Aikens, C. M. Theoretical Analysis of the Optical Excitation Spectra of Silver and Gold Nanowires. *Nanoscale* **2012**, *4*, 4190−4198.
(44) Swasey, S. M.; Karimova, N.; Aikens, C. M.; Schultz, D. E.; Simon, A. J.; Gwinn, E. G. Chiral Electronic Transitions in Fluorescent Silver Clusters Stabilized by DNA. *ACS Nano* **2014**, *8*, 6883−6892.

https://doi.org/10.1021/acs.jpcc.3c04103
J. Phys. Chem. C XXXX, XXX, XXX−XXX